JOINT EUROPEAN TORUS

JET–P(92)44

K. Borrass, D. Campbell, S. Clement, G. Vlases
and JET Team

Scrape-Off Layer Based Modelling of the Density Limit in Beryllated JET Limiter Discharges

Scrape-Off Layer Based Modelling of the Density Limit in Beryllated JET Limiter Discharges

K. Borrass[1], D. Campbell, S. Clement, G. Vlases
and JET Team*

JET-Joint Undertaking, Culham Science Centre, OX14 3DB, Abingdon, UK

[1]NET Team, Max-Planck-Institut ftir Plasmaphysik, Garching bei Mtinchen, Germany
** See Annex*

Preprint of Paper to be submitted for publication in
Nuclear Fusion

SCRAPE-OFF LAYER BASED MODELLING OF THE DENSITY LIMIT IN BERYLLATED JET LIMITER DISCHARGES

K. BORRASS
NET Team, Max-Planck-Institut für Plasmaphysik,
Garching bei München,
Federal Republic of Germany

D. CAMPBELL, S. CLEMENT, G. VLASES
JET Joint Undertaking,
Abingdon, Oxfordshire,
United Kingdom

ABSTRACT. This paper gives a scrape-off layer based interpretation of the density limit in beryllated JET limiter discharges. In these discharges JET edge parameters show a complicated time evolution as the density limit is approached and the limit is manifested as a non-disruptive density maximum which cannot be exceeded by enhanced gas puffing. The occurrence of marfes, the manner of density control and details of recycling are essential elements of the interpretation. Scalings for the maximum density are given and compared with JET data. The relation to disruptive density limits, previously observed in JET carbon limiter discharges, and to density limits in divertor discharges is discussed.

1. INTRODUCTION

In the present paper, the density limit (DL) in JET beryllium limiter discharges is investigated. In a series of DL discharges, run on the beryllium belt limiter with a beryllium evaporation coating on the walls, it was found that a DL occurred, being manifested as a resistance to further density increase, irrespective of the strength of gas puffing (refuelling limit). The limit always coincided with the appearance of a marfe [1]. A distinguishing feature of these discharges was that they were almost never disruptive, and in many cases the marfe would extinguish, after which the bulk plasma density would recover to its pre-marfe value, and the entire cycle would be repeated one or more times. Figure 1 shows an example of such behaviour. It was further shown that the DL was associated with the edge density rather than the line averaged density [1], similarly to findings in ASDEX DL studies [2].

The refuelling limit seen in JET is illustrative of one of several physical mechanisms which may limit tokamak densities. Basically one has to distinguish between the classical disruptive density limit (DDL), where the discharge is terminated by a disruption when a certain critical density is exceeded, and non-disruptive density limits (NDLs), which are manifested as bounds of the accessible density space. A second important distinction is between cases where the plasma is detached and cases where the plasma has full limiter/plate contact when the limit is reached. In the latter case the limit typically seems to be a limit of the edge density [1, 2]. Essentially all cases are found in experiment: In a typical disruptive limiter discharge, a radiating layer with a cold plasma edge (detached plasma) develops, which leads to shrinking of the current channel and subsequent destabilization of the $m/n = 2/1$ mode [3] (DDL without limiter contact). In divertor discharges the situation may be different, and the plasma may be in full contact, at least with the outboard target plates, when the disruption occurs [4] (edge DDL with plate contact). Finally, the JET refuelling limit to be analyzed in this paper is a non-disruptive limit

where the plasma has full limiter contact at the limit (edge NDL with limiter contact).

There are characteristic differences in the physics underlying the various DLs which impact on the possible approaches to a theoretical description. For cases where the plasma is detached when the DL is reached, the scrape-off layer (SOL) does not play a role, and the density limiting mechanism is entirely determined by bulk plasma physics. If, on the other hand, the plasma is in contact with the limiter/plate and the limit is an edge limit, the edge density can be determined by solving the SOL equations. Of course, a fully self-consistent description of the plasma boundary requires a coupled model describing both the bulk and SOL plasmas. However, a purely SOL-based analysis of the problem is possible if the boundary conditions at the separatrix/last closed flux surface[1] are known. Within the framework of a 1-D analysis, which contains all the essentiall elements of the problem, the only boundary condition which is needed is the power flux across the separatrix, which can be taken directly, or inferred, from experiment. Thus, while this approach is inherently incomplete, it may provide important information, such as the maximum achievable edge densities, in a situation where a fully self-consistent treatment is not available.

Limits on the edge density have assumed an increasingly important role in the design of next step devices. For example, conceptual design work for NET and ITER has yielded clear evidence that divertor design limitations impose conditions on the divertor plasma which can ultimately be translated into a minimum acceptable edge density [5, 6], and may thus be in conflict with egde DLs.

In the present paper the JET refuelling limit is interpreted along these lines. In Ref. [7] a SOL-based model was proposed for the disruptive limit in an ADEX-type divertor configuration and tested against the ASDEX DL database. In this paper, we use a version of the SOL model of Ref. [7] modified to describe limiter plasma discharges. Although the modifications are relatively minor, they result in a qualitatively and quantitatively different picture of the density limiting mechanisms, as compared with the model for divertor limits. We interpret the existence of an edge density maximum as being caused by the appearance of a marfe and specific

[1]For convenience the term separatrix is applied to both cases in the following.

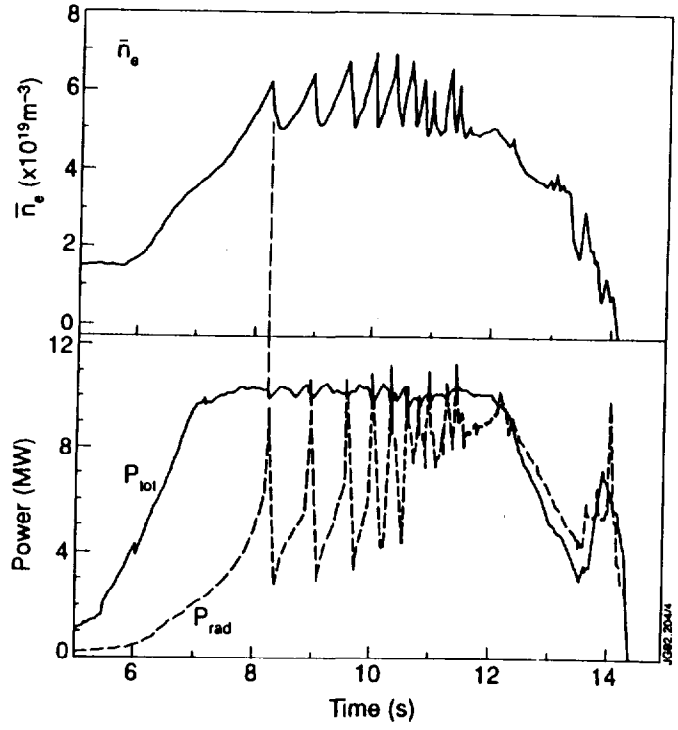

FIG. 1. *The density and radiated power oscillation during a typical beryllium limiter density limit discharge.*

refuelling characteristics. The repetitive nature of this process and the resistance of the maximum to refuelling enhancement are also discussed. The distinction between these discharges and the JET "carbon machine" DDL discharges described by Wesson et al. [3] is briefly considered.

2. DESCRIPTION OF SOL MODEL

The two-point analytical SOL model of Ref. [7], originally formulated for ASDEX-type divertor configurations, has been extended to limiter cases by (1) assuming $L = L_s$ (L: total connection length, L_s: connection length to the X-point), (2) extending the model to allow for arbitrary poloidal distributions of the power flux across the separatrix and (3) appropriately modifying the recycling model. Limiter configurations are thus treated as special divertor configurations.

2.1 Basic model equations

The distribution of the power flux $q_\perp$ across the separatrix essentially determines the ratio of n_S (stagnation point density) and n_D (limiter

density) (and correspondingly, because of the pressure balance, that of T_S and T_D). The close link to the bulk plasma in limiter discharges will generally prevent strong gradients along the field lines, but due to the strong recycling around the limiter a moderate temperature drop towards the limiter has to be expected, while n_S and n_D will be of similar size. Within the model this is obtained if a poloidally constant power flux across the separatrix is assumed. The TEXTOR limiter tokamak has the diagnostic capabilities to perform simultaneous measurements of n_S and n_D (or T_S and T_D). No systematic analysis has been reported, but the assumption of a constant flux seems to be consistent with TEXTOR observations [8].

With these specifications the basic equations of Ref. [7] take the form[1]

$$n_D = \frac{n_S T_S}{2T_D} \tag{1}$$

$$\Delta = \frac{5}{32}\frac{c}{e}\frac{\alpha_{D_B} n_S T_S^2}{q_\perp B_t} \tag{2}$$

$$T_S = \left(\frac{49}{4\kappa}\frac{\alpha_{q_\perp} q_\perp L^2}{\Delta}\right)^{2/7}\left(1-\left(\frac{T_D}{T_S}\right)^{7/2}\right)^{-2/7} \tag{3}$$

$$\frac{7}{2}\frac{Lq_\perp}{\Delta_E} = \xi(1-P_{exh})c_s(T_D)n_D + \int_0^L dz Q_{imp} + \gamma T_D c_s(T_D) n_D \tag{4}$$

Here Δ and Δ_E are the temperature and power SOL thicknesses, respectively. $q_\perp$ is the mean power flux across the separatrix. ξ and γ are the mean ionization energy of neutrals and the sheath transfer coefficients, respectively. P_{exh} is the exhaust probability of a recycling neutral, and $c_s(T_D)$ is the ion sound speed. $\alpha_{q_\perp}$ characterizes the poloidal distribution of $q_\perp$; $\alpha_{q_\perp} = 1/2$ for the choice made for the power flux distribution [7]. Bohm diffusion is adopted for perpendicular SOL transport ($\alpha_{D_B} = 1$).

Equation (1) is derived from the momentum balance equation. Equations (2) and (3) follow from local analysis of the SOL power balance, while Eq. (4) is essentially the global power balance equation at the target. The terms on the right-hand side of Eq. (4) are the loss terms associated with ionization and impurity radiation and with the power flux into the sheath region. For detailed discussion of Eqs (1) to (4) see Ref. [7].

[1]The units are *cgs* units except where otherwise stated.

In Eq. (4) we have suppressed several terms which are mainly associated with the energy transfer by neutrals and approximately cancel. On the assumption that most neutrals perform at least one charge exchange reaction before hitting the wall (this being a natural assumption for typical limiter shapes), these terms would be

$$c_s(T_D)n_D\left[\frac{3}{2}T_D - 6T_D\frac{R_E(6T_D)}{R_N(6T_D)} + \frac{3}{2}T_D(1-P_{exh}) + 2T_D P_{exh}\left(1-\frac{R_E(T_D)}{R_N(T_D)}\right)\right] \tag{5}$$

Here the first two terms describe the energy transferred to the SOL plasma by neutrals coming from the limiter during their first charge exchange reaction. The incident energy of an ion hitting the plate is $E_i = 6T_D$ [9], and $E_i R_E/R_N$, where R_E and R_N are the energy and particle reflection coefficients, is the mean energy of a neutral coming from the plate [10]. The third term describes the energy needed to heat the electrons up to the local temperature T_D after ionization and the last term is associated with the power transfer of neutrals to the wall. Typically one has $R_E/R_N \simeq 0.5$, independently of incident energy [10]. For the P_{exh} values occurring in this study ($P_{exh} \leq 0.3$) the contribution from Eq. (5) therefore lies between $-0.4c_s(T_D)n_D T_D$ and 0 and is only a small correction to the last term of Eq. (4) ($\gamma \simeq 8$) and can conveniently be ignored.

A more convenient form of Eq. (4) has been derived in Ref. [7]:

$$n_S = \left(\frac{7}{c_s}\right)^{11/16}\left(\frac{32e}{5c}\frac{1}{\alpha_{D_B}}\right)^{5/16}\left(\frac{4\kappa}{49}\frac{1}{\alpha_{q_\perp}}\right)^{3/8} \times \frac{B_t^{5/16} q_\perp^{5/8}}{L^{1/16}}\left[1-\left(\frac{T_D}{T_S}\right)^{7/2}\right]^{3/8} \times \frac{T_D^{11/32}}{\left\{\xi(1-P_{exh}) + \frac{\int_0^L dz Q_{imp}}{\tilde{c}T_D^{1/2}} + \gamma T_D\right\}^{11/16}} \tag{6}$$

where $c_s(T_D) = \tilde{c}T_D^{1/2}$. In many cases all other dependences except the explicit T_D-dependence can be approximately ignored in the right-hand side of Eq. (6), and one has an explicit expression for n_S versus T_D which gives some insight into the general solutions of Eqs (1) to (6), which are otherwise rather implicit.

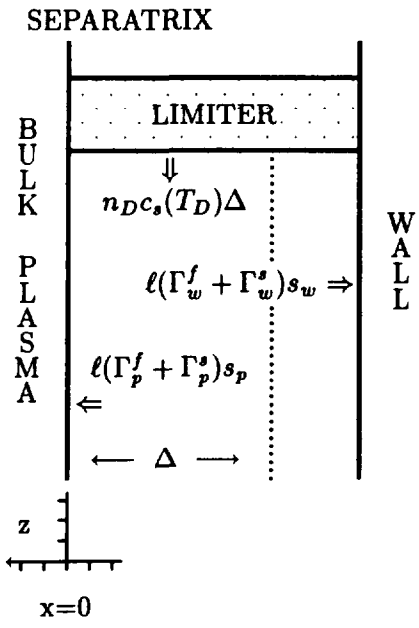

FIG. 2. *Slab model for recycling in a limiter configuration (poloidal cross-section view). l is the characteristic length of the recycling zone.*

Other SOL related quantities can be expressed in terms of the basic variables n_D, T_D, Δ, T_S and n_S. An important derived parameter in the following discussion is the gas throughput, which, within the model, is given by

$$\dot{N} = 2\pi R_D n_D c_s(T_D)\Delta P_{exh} \tag{7}$$

where R_D is the plate/limiter radius.

2.2 Recycling

Recycling is described by P_{exh} in Eqs (4) and (6). A slab model according to Fig. 2 which includes fast and slow neutrals is used to evaluate P_{exh}. The particle balance for fast neutrals in the region under consideration gives

$$n_D c_s(T_D)\Delta = \ell[\Gamma_p^f s_p + \Gamma_w^f s_w + \Delta n_D n_0^f S_i + \frac{1}{2}\Gamma_w^f - \Gamma_p^s(1-s_p)] \tag{8}$$

The left-hand side is the flux of neutrals coming from the limiter. On the right-hand side, the first two terms are fluxes of fast neutrals which are "pumped" by the bulk plasma and the wall, respectively. s_p and s_w are the respective sticking probabilities. The third term describes ionization of fast neutrals in the SOL. S_i is the ionization rate for atomic hydrogen. About 50% of the fast neutrals hitting the wall are reflected with nearly full energy, while the rest are converted into slow neutrals which return as molecules with an energy corresponding to the wall temperature [10]. This sink for fast neutrals is described by the fourth term. Slow neutrals hitting the bulk plasma are absorbed or reflected. In the latter case they have performed at least one charge exchange reaction and hence return as fast neutrals. This source of fast neutrals is described by the fifth term.

By analogy one obtains for the slow neutrals the balance equation

$$\frac{1}{2}\ell\Gamma_w^f = \ell[\Gamma_p^s + \Gamma_w^s s_w + \Delta n_D n_0^s S_i] \tag{9}$$

Here it is implicitly assumed that low-energy molecular hydrogen essentially dissociates in the temperature range of interest [11].

Adding Eqs (8) and (9) yields

$$n_D c_s(T_D)\Delta = \ell[(\Gamma_p^f + \Gamma_p^s)s_p + (\Gamma_w^f + \Gamma_w^s)s_w + \Delta n_D n_0^f S_i] \tag{10}$$

In order to evaluate the particle fluxes, the distributions of fast and slow neutrals have to be known. For fast neutrals we take

$$f^f = \frac{2}{3}n_0^f(f_M(T_D) + f_M^+(T_D)) \tag{11}$$

where f_M is a Maxwellian and $f_M^+ = f_M(\Theta(V_x)V_x, V_y, V_z)$. This ansatz takes into account the annihilation of 50% of fast neutrals at the wall. For slow neutrals we assume a Maxwellian distribution with energy 2.2 eV [12]

$$f^s = n_0^s f_M(2.2\ eV) \tag{12}$$

For the fluxes one now gets $\Gamma_p^f = 1/6 V_0^f n_0^f$, $\Gamma_w^f = 1/3 V_0^f n_0^f$, $\Gamma_p^s = 1/4 V_0^s n_0^s$ and $\Gamma_w^s = 1/4 V_0^s n_0^s$, where $V_0^{f/s}$ are the mean velocities of fast and slow neutrals, respectively. With this information Eq. (9) provides a relation between n_0^f and n_0^s

$$n_0^f = \frac{3}{2}n_0^s \frac{V_0^s}{V_0^f}\left(1 + s_w + \frac{4\Delta}{\lambda_i^s}\right) \tag{13}$$

where λ_i^s is the ionization mean free path for slow neutrals.

Finally, after some elementary algebra, one gets from Eqs (10) and (13)

$$P_{exh} = \frac{\ell(\Gamma_w^f + \Gamma_w^s)s_w}{\Delta n_D c_s}$$

$$= \frac{1}{1 + \frac{1+\rho}{1+2\rho}\frac{s_p}{s_w} + \frac{4+6\rho V_0^s/V_0^f}{1+2\rho}\frac{1}{s_w}\frac{S_i \Delta n_D}{V_0^s}} \quad (14)$$

where $\rho = 1 + s_w + \Delta S_i n_D / V_0^s$.

For the beryllated JET discharges considered in this study $s_w = 0.1$ is adopted. s_w is nearly independent of the energy and angle of incidence, and hence the same value can be taken for fast and slow neutrals.

In order to estimate s_p, we consider a beam of neutrals with a mean velocity V_0 corresponding to T_D which enter the bulk plasma in the x-direction. They diffuse under the influence of charge exchange reactions and ionization according to (see Ref. [7])

$$-\frac{\partial}{\partial x}\left(D_0 \frac{\partial n_0}{\partial x}\right) + n_D n_0 S_i = 0 \quad (15)$$

where $D_0 = 1/3 V_0 \lambda_{cx}$ and λ_{cx} is the mean free path for charge exchange reactions. (For the origin of the factor 1/3 see, for instance, Ref. [13] and note that charge exchange neutrals have an isotropic angular distribution in the laboratory frame.). With constant temperature $T = T_D$ assumed, Eq. (15) has the solution

$$n_0(x) = n_0 e^{-x/\lambda} \quad (16)$$

where $\lambda^2 = 1/3 \lambda_{cx} \lambda_i$ and λ_i is the mean free path for ionization [7]. It thus follows that

$$s_p = -D_0 \frac{\partial n_0(0)}{\partial x} \ell \Big/ V_0 n_0 \ell = \frac{1}{\sqrt{3}} \sqrt{\frac{S_i(T_D, n_D)}{S_{cx}(T_D)}} \quad (17)$$

A neutral particle adopts the energy corresponding to the local temperature after its first charge exchange reaction. This justfies the use of s_p according to Eq. (17) for fast and slow neutrals that was made in the above consideration.

In Fig. 3, P_{exh} is given versus T_D for two extreme densities and a typical SOL thickness, which illustrates that it is essentially a function of temperature. The sharp increase of P_{exh} for temperatures below about 10 eV is due to the strong decrease of the ionization rate S_i in this regime [12].

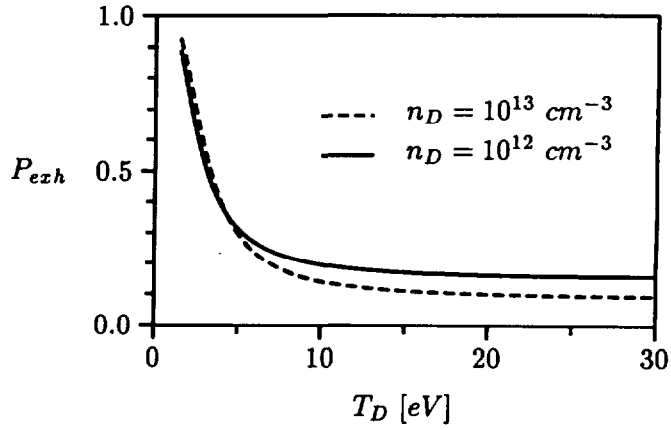

FIG. 3. *Exhaust probability P_{exh} versus T_D for two different densities. $s_w = 0.1$ and $\Delta = 2$ cm in both cases. For S_i and S_{cx} the model expressions of Ref. [7] are used.*

2.3 Impurity radiation in the SOL

The discussion of impurity radiation in the SOL is based on a simple model proposed in Ref. [7] for the ASDEX tokamak. It reflects the fact that in the presence of typical medium-Z, recycling impurities, radiation comes from a thin layer of thickness ℓ in front of the plate/limiter and that, for not too low temperatures, $Q_{imp} \propto n_e n_{imp}$ holds, independently of temperature. Hence in this approximation one has

$$\int_0^L dz Q_{imp} \propto \gamma_{imp} n_D^2 \ell \quad (18)$$

where γ_{imp} is the impurity concentration.

The width ℓ of the radiating zone should be independent of the configuration and there is also no indication of impurity concentrations in a limiter SOL being considerably higher than in a divertor SOL. However, the densities at the limiter in the JET discharges are much lower than the divertor densities in comparable ASDEX discharges (see, for instance, Table I below and Table II of Ref. [7]). This is elucidated by the scaling of n_D with respect to $L, q_\perp, T_D$ and $\alpha_{q_\perp}$,

$$n_D \propto \frac{L^{5/16} q_\perp^{7/8}}{T_D^{41/32} \alpha_{q_\perp}^{1/8}} \quad (19)$$

which is obtained from Eqs (1) to (4) by retaining only the dominant third term in Eq. (4) and

assuming $(1 - (T_D/T_S)^{7/2})^{-2/7} \simeq 1$. There is only weak impact from the difference in L and $\alpha_{q_\perp}$. However, the T_D values at the limit are typically somewhat higher in JET ($\approx$ 10 eV, see below) than in ASDEX ($\approx$ 5 eV, see Ref. [7]). Also $q_\perp$ is lower in JET than in ASDEX. While typical ratios P_{heat}/O_{plasma} (O_{plasma} the plasma surface) are similar, the bulk plasma radiative fraction near the limit is much higher in JET discharges under consideration ($\approx$ 75%) than in ASDEX divertor discharges ($\approx$ 40%, see Ref. [14]).

In ASDEX impurity radiation provides only a small fraction of the energy account in the SOL [7], which is further reduced in JET by more than an order of magnitude. Impurity radiation losses in the SOL are therefore completely negligible in the present analysis.

Though small, impurity radiation losses are an essential element in the model proposed in Ref. [7] for the DDL in ASDEX. The further drastic reduction of these losses in JET is one reason why this mechanism is not effective in JET (and probably other limiter discharges). These aspects will be reconsidered in Sec. 6.

2.4 Options for solving the basic equations

With P_{exh} from Eq. (14), Eqs (1) to (4), plus definition equations for, say, n derived quantities, provide $4 + n$ equations for the $6 + n$ variables n_S, T_S, n_D, T_D, Δ, $q_\perp$ and the n derived quantities. Any two of them can be specified to determine the rest. In this study the following four options are applied:

(i) n_D and T_D are given, while $q_\perp$, n_S, T_S, $\dot{N}$, etc. are calculated. This option is used to interpret limiter probe measurements of n_D and T_D.

(ii) $q_\perp$ and n_S are given. This option is used to describe the slow, quasi-steady-state density ramp-up phase, when the radiated power (and hence $q_\perp$ for given heating power) is essentially a function of n_S (see Sec. 2.5).

(iii) $\dot{N}$ and $q_\perp$ are given. This option is used to describe the marfing phase, when one has typically decreasing $q_\perp$ at constant $\dot{N}$.

(iv) $q_\perp$ and T_D are given. For sufficiently high T_D so that $P_{exh} << 1$, Eqs (1), (2), (3) and (6) can be approximately solved in terms of these variables. This feature will be used to derive scaling relations for n_S^{max} in terms of conventional global parameters from Eq. (6).

2.5 Bulk radiation

In terms of external parameters, $q_\perp$ is given by

$$q_\perp = \eta \frac{P_{in}}{4\pi^2 a R \sqrt{\kappa}} \tag{20}$$

where κ is the plasma elongation and η takes into account asymmetries in the distribution of the power flux between the inner and outer divertor channels as observed in experiments. $P_{in} = P_{heat} - P_{rad} - \dot{W}$ is the power to the SOL. Throughout the rest of the paper we take $\dot{W} \simeq 0$ so that P_{in} is also the net input power to the bulk plasma. This approximation is certainly justified during the quasi-steady-state ramp-up phase. After the onset of marfes a small boundary zone shows rapid variation (see Sec. 3), but it contains only a small fraction of the internal energy. Direct measurement of $\dot{W}$ supports this approximation.

Within the SOL model n_S and $q_\perp$ (or equivalently P_{in}) are independent parameters. In a real discharge, it is the time evolution of P_{heat} which is explicitly prescribed, while P_{rad} evolves self-consistently. Under quasi-steady-state conditions P_{rad} is mainly a function of density. This relation between density and $q_\perp$ provides an additional constraint for the SOL solution space.

A simple, widely accepted model for the power radiated under quasi-steady-state conditions from the bulk plasma layer is

$$P_{rad} \simeq C_{rad}(Z_{eff} - 1)n_S^2 \tag{21}$$

where Z_{eff} is some mean value and C_{rad} depends on the device parameters and the dominant impurity. Equation (21) implicitly assumes a stiff correlation between the density at the first or second radiation maximum of the dominant impurity and n_S (profile consistency). When calibrated with bolometric measurements Eq. (21) gives a reasonable fit for the class of discharges considered in this study ($C_{rad} = 9.6 \times 10^{-26}$ $[MWcm^6]$). Of course, this simple model breaks down when marfes occur or when the situation is no longer quasi-steady-state.

It is frequently observed that $Z_{eff} - 1$ decreases linearly with increasing density during a discharge, corresponding to an approximately constant impurity content. Hence one has also

$$P_{rad} \simeq \tilde{C}_{rad} n_S \tag{22}$$

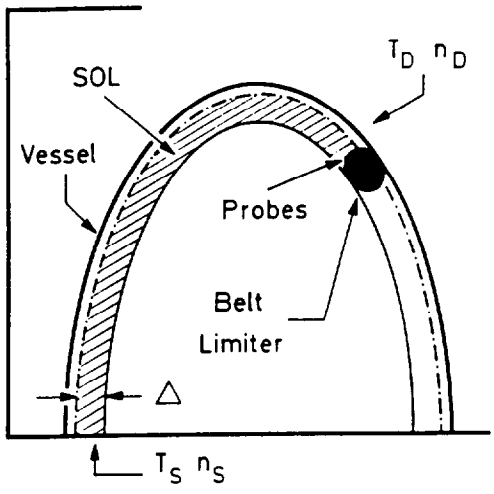

FIG. 4 *Position of JET belt limiters and limiter Langmuir probes (schematic). The hatched area indicates the part of the SOL considered.*

where $\tilde{C}_{rad}$ is in general discharge dependent. Equation (22) is a relatively crude approximation which is only used for illustrative purpose.

3. EMPIRICAL DATABASE AND MODEL VALIDATION

The present study is based on a series of forty JET pulses which form a database for density limit studies carried out using the solid beryllium belt limiter and beryllium evaporation. These discharges covered a wide range of plasma parameters: $1.2\ MA \leq I_p \leq 4\ MA$, $2\ MW \leq P_{heat}\ (Ohmic + NI + ICRH) \leq 21\ MW$, $1.7 \leq q_{cyl} \leq 6.5$, and toroidal field strengths of 1.5 T, 2.3 T and 2.6 T. The general features of these discharges were discussed in Ref. [1].

Extensive use is made of data from Langmuir probes located in the belt limiter facing towards the inboard SOL (Fig. 4), which, due to asymmetric power distribution between the inboard and outboard channels, determines the density limit in edge based models [7]. We begin by examining in detail the temporal behaviour of the edge parameters of a particular discharge and show that all the features observed in the experiment are described quantiatively by the model.

Figure 5 shows the time evolution of edge and related parameters for a typical JET limiter discharge in the vicinity of the DL. The periodic behaviour will be considered below. When, for instance, the first period (t = 48 s to t = 49.5 s) is taken, the following observations can be made:

(1) The radiated power increases monotonically at nearly constant input power. Hence the power flux $q_\perp$ into the SOL decreases monotonically.
(2) The plasma temperature at the limiter decreases continuously.
(3) The plasma density at the limiter runs through a maximum (at t = 48.8 s).
(4) More detailed inspection also shows that marfing starts when the limiter density reaches maximum.
(5) After the onset of marfing the gas throughput stays approximately constant.

When modelling this behaviour one is faced with the problem that, while the probe data n_D and T_D directly refer to the SOL under consideration, only the total gas throughput $\dot{N}_{tot}$ and the total power crossing the separatrix are measured. Instead of using $\dot{N}_{tot}$ and P_{in} as input for modelling, we therefore start with measured values of n_D and T_D (triangles (△) in Figs 5 a) and 5 b)) for the six points P_1 to P_6. In a first step the model equations give $q_\perp$ and $\dot{N}_{in}$ for the inboard channel under consideration. The value obtained for $q_\perp$ for the third point P_3 (at t = 48.7 s), which is close to the maximum, is then used to determine η_{in}, where η describes deviations of $q_\perp$ from its mean value as discussed in Sec. 2.5. One obtains η_{in} = 0.214. For the fraction $\mu_{in} = \dot{N}_{in}/\dot{N}_{tot}$ of gas going into an inboard channel we assume μ_{in} = 0.25, i.e. equal fractions of the gas throughput are attributed to all four channels, which gives a good overall fit of $\dot{N}_{tot}$. It is assumed that η_{in} and μ_{in} are discharge independent and the above numbers are used throughout the rest of the paper. We also use these relations to replace the variables $q_\perp$ and $\dot{N}_{in}$ by the more intuitive global quantities P_{in} and $\dot{N}_{tot}$ in figures and tables. In order to establish the relation between $q_\perp$ and P_{rad}, we use $P_{in} = P_{heat} - P_{rad}$ and the experimental values for $P_{heat}(t)$ (see Fig. 5 e). The calculated values for P_{rad} and $\dot{N}_{tot}$ obtained in this way reproduce the measured time evolution reasonably well ((+) in Figs c) and d).

Table I summarizes the modelling results for points P_1 to P_6 of this series, including parameters for which no direct experimental information is available. Most important is that the stagnation point and limiter densities behave similarly. Generally, because the connection length is comparatively short and the poloidal distribution of $q_\perp$ is flat, T_S and n_S are closer to T_D and n_D in

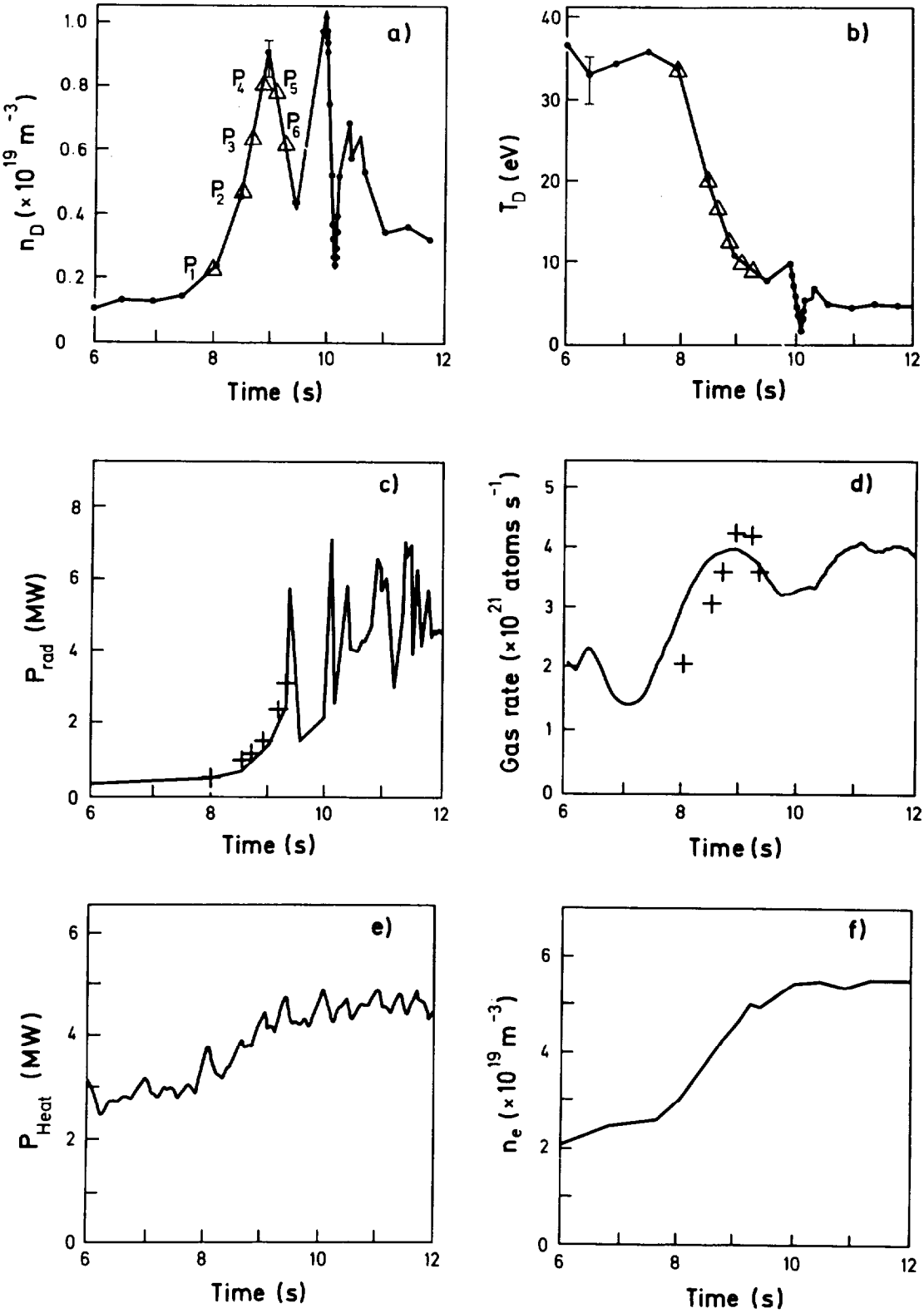

FIG. 5. *Time evolution of relevant parameters close to the density limit of shot 20845. Discharge parameters are: NBI power 4.7 MW, $q_c = 2.22$ and $B_t = 2.59$ T. + denotes values of P_{rad} and $\dot{N}$ calculated with measured values ($\triangle$) of n_D and T_D.*

(a) Limiter density (probe data) *(b) Limiter temperature (probe data)*
(c) Total radiation (bolometric measurement) *(d) Total gas consumption*
(e) Heating power *(f) Line average density*

Dots in Figs (a) and (b) represent an average of four measurements. An exception is the interval between 9.9 s and 10.15 s, where a high sampling rate has been used (see also Fig. 6).

TABLE I. MODELLING OF SHOT 20845[a]

		P_1	P_2	P_3	P_4	P_5	P_6
n_D	$[10^{12}cm^{-3}]$	2.1	4.7	6.3	8.0	7.8	6.2
T_D	$[eV]$	34	20	17	13	10	8.8
n_S	$[10^{12}cm^{-3}]$	4.0	6.7	7.6	7.9	6.6	5.3
T_S	$[eV]$	37	28	27	25	23	21
P_{exh}		0.14	0.13	0.13	0.14	0.16	0.19
$\dot{N}_{tot}$	$[10^{21}at/s]$	2.1	3.0	3.6	4.3	4.2	3.6
P_{in}	$[MW]$	2.5	2.5	2.5	2.3	1.6	1.1
P_{rad}	$[MW]$	0.51	1.0	1.1	1.5	2.4	3.0

[a] Measured values for n_D and T_D (first two rows) are used to calculate the other quantities of the table. $\dot{N}_{tot}$ and P_{in} are related to $\dot{N}_{in}$ and $q_\perp$ as outlined in Sec. 3.

limiter discharges than in comparable divertor cases, respectively.

Information about the power and particle distribution is very limited. The value of $\mu_{in} = 0.25$ is a natural guess. η_{in} can be related to the outboard/inboard power distribution ratio. From $\eta_{in}g_{in} + \eta_{out}g_{out} = 1/2$, where $g_{in/out}$ are the fractions of the separatrix linked to an inboard/outboard SOL, respectively, one gets η_{out}. For an arrangement according to Fig. 4 with $g_{in} \simeq 1/3$ and $g_{out} \simeq 1/6$, $\eta_{out} = 2.57$ is obtained. With these numbers, the outboard/inboard power distribution ratio $\eta_{out}g_{out}/\eta_{in}g_{in}$ is 6.

Limitations in data handling restrict the sampling rate of routinely performed probe measurements. For special reasons a particularly high sampling rate was applied in the second period of Fig. 5 (9.9 s to 10.15 s), which is expanded in Fig. 6. In this case modelling is done differently. In order to avoid any assumption on η, we calculated n_D (+ in Fig. 6 b)) for various values of T_D ($\triangle$ in Fig. 6 a)) and constant $\dot{N}_{tot} = 4.2 \times 10^{21}\ at/s$ taken from the preceding example. The agreement is again remarkably good.

4. DISCUSSION

Now that the potential of the model to describe the SOL has been demonstrated, it can be used as a basis for a more systematic discussion. As a first step we consider n_S as a function of P_{in} and $\dot{N}_{tot}$ ($n_S = n_S(P_{in}, \dot{N}_{tot})$). In Fig. 7, various calculated $\dot{N}_{tot} = const$ curves, the bulk radiation constraint according to Eq. (22) for two different fixed heating

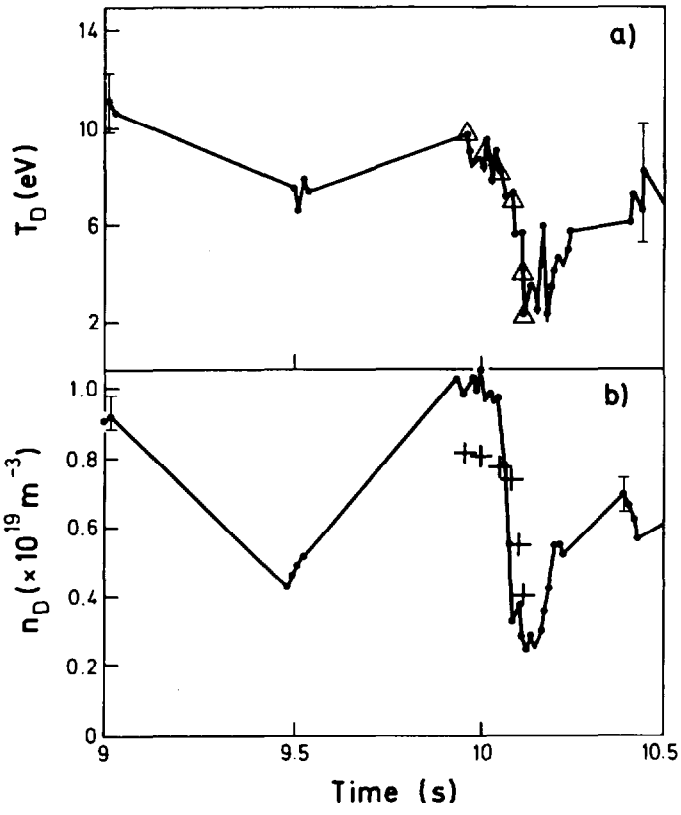

FIG. 6. *Expanded view of the second period of the shot shown in Fig. 5. + denotes values of n_D calculated from measured values of T_D ($\triangle$) at $\dot{N}_{tot} = 4.2 \times 10^{21}\ at/s$*

powers, and the trajectory of shot 20845 are plotted in the n_S-P_{in} plane.

During the density ramp-up phase, when quasi-steady-state conditions prevail, one moves along the bulk radiation constraint. In Fig. 7 the radiation constraint is given for fixed values of P_{heat}. Actually, it differs from this simple straight line form since P_{heat} varies somewhat during the discharge (see Fig. 5 d)). Curves with growing $\dot{N}$ are crossed in this phase. A continuous increase of the gas rate during density ramp-up is generally observed in experiments. This behaviour is not simply a consequence of the increase of the plasma particle contents. Indeed, almost all gas is pumped during the recycling process, the fraction going into the plasma being negligible. The increase of the gas rate instead reflects the increase of P_{exh} resulting from the decreasing plasma temperature at the limiter (see Table I and Fig 3).

When marfing starts ($t = 49\ s$), a sizable fraction of radiation is determined by the (poloidally localized) density of the marfe. Furthermore, steady-state conditions no longer prevail in the bulk plasma boundary. Hence radiation becomes decoupled from n_S. We know, however, from experiment that P_{rad}

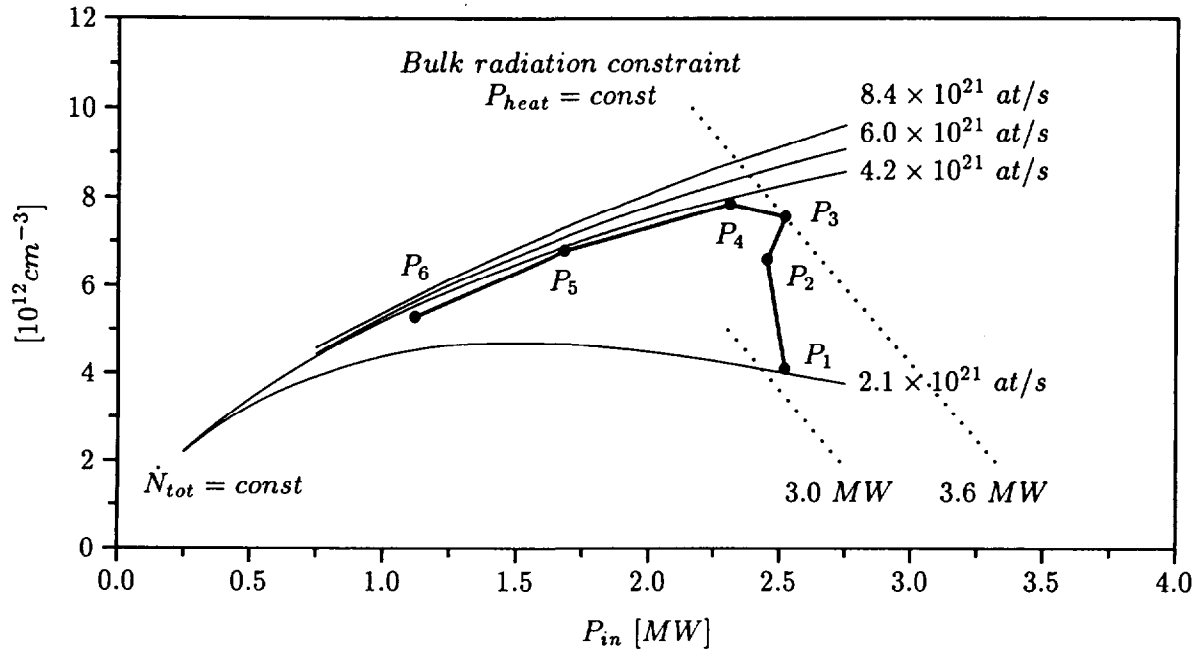

FIG. 7. *Illustration of the mechanism leading to a maximum density. All data result from simulations of shot 20845. Thin solid curves: curves of constant gas throughput $\dot{N}_{tot}$. Dotted curves: bulk radiation constraint according to Eq. (22) for constant heating powers $P_{heat} = 3.0$ MW (heating power in P_1) and $P_{heat} = 3.6$ MW (heating power in P_3). Thick solid curve: trajectory of shot 20845 (same time interval as in Fig. 5). • are the points considered in Table I.*

continues to increase and hence $q_\perp$ continues to decrease, while $\dot{N} \simeq const$ follows from the way in which density control is operated. Hence, after the onset of marfing one moves along the $\dot{N} = const$ curve in Fig. 7, which is defined by the $\dot{N}$ value prevailing at this moment, and n_S decreases.

According to this picture the density maximum should therefore coincide with the onset of marfes, as is actually seen in experiment. The threshold condition for marfes is reached when locally the temperature falls to near the value of the first or second radiation peak of the predominantly radiating impurity. This is typically the case for limiter temperatures in the 10 eV range. We therefore come to the conclusion that the maximum is achieved for values of T_D in this range (see Fig. 5 and Ref. [15]).

The maximum of n_S, resulting in the way described, is associated with a discontinuity in $\partial n_S / \partial q_\perp$ as indicated on Fig. 7. Even though the experimental resolution is limited, Fig. 5 seems to support this.

One might suspect that the density maximum simply reflects the special manner of density control adopted, and that enhanced gas throughput would help to maintain n_S at its maximum value or even raise it. Figure 7 clarifies this. For $\dot{N}$ values above the actual value of $\dot{N}_{tot} = 4.2 \times 10^{21}$ the $\dot{N}_{tot} = const$ curves become very narrowly spaced. Hence even a slight increase of n_S requires drastic increases of the fuelling rate. This is experimentally observed and has been described as refuelling limit [16].

The gas throughput $\dot{N}$ is basically determined by the exhaust probability $P_{exh}(T_D)$ (see Eq. (7)), and the refuelling limit must be associated with a strong increase of P_{exh}. To elucidate the mechanism, we now consider n_S as a function of T_D and $q_\perp$ (or equivalently P_{in}) ($n_S = n_S(T_D, q_\perp)$) and illustrate the situation in the n_S-T_D plane as shown in Fig. 8. For constant P_{in}, the dependence of n_S on T_D is only very weak and a slight increase of n_S is associated with a strong decrease of T_D, which increases P_{exh}. The effect becomes particularly pronounced below about 10 eV, where P_{exh} depends sensitively on temperature (see Fig. 3). According to the picture outlined, the refuelling resistance and the existence of an edge density maximum have separate causes and their simultaneous occurrence at limiter temperatures of about 10 eV is accidental.

We can now offer a qualitative explanation of the cyclic behaviour of the edge parameters. The basic element is that the rapid decay of the edge density after the onset of the marfe ultimately reduces the

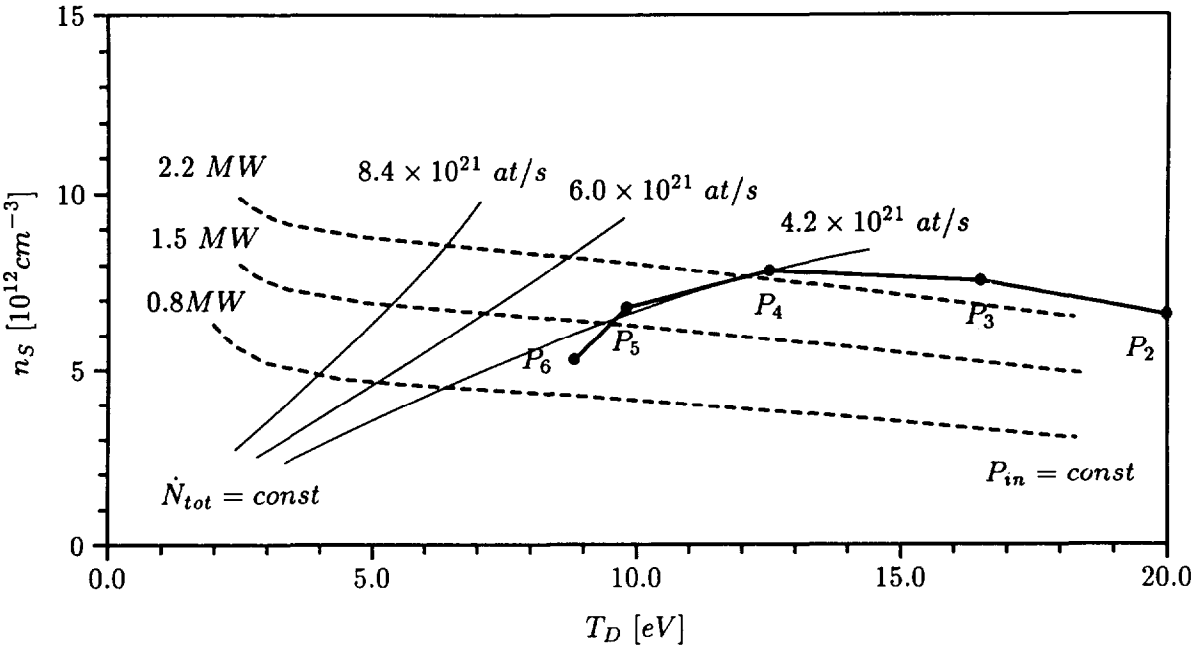

FIG. 8. *Projection of the SOL solution space into the n_S-T_D plane. All data result from simulations of shot 20845. Thin solid curves: curves of constant $\dot{N}_{tot}$. Dashed curves: curves of constant P_{in}. Thick solid curve: trajectory of shot 20845. • are the points considered in Table I.*

density at the marfe radius below the threshold for the onset of marfes. Once the extra radiation of the marfe disappears, $q_\perp$ increases and n_S can recover. The processes under consideration occur on a time scale much shorter than the bulk particle confinement time and therefore strong deformation of the density profile near the edge has to be expected and the marfe feels the variation of n_S with a certain delay. This makes it difficult to identify the precise path in, for instance, Fig. 7. It is, however, confirmed by experiment that marfes periodically disappear and that the onset continues to coincide with the edge density maxima.

5. SCALING RELATIONS

For practical applications there is a need for simple scaling-type relations for n_S^{max} in terms of global discharge parameters (a, R, κ, B_t, q) and the net input power P_{in}. These can be conveniently derived from Eq. (6) by applying the conclusions of the preceding discussion. From Sec. 4 we know that $T_D^{max} \simeq 10\ eV$, where T_D^{max} is the divertor temperature for which $n_S = n_S^{max}$. In this temperature range we have $(1 - (T_D/T_B)^{7/2})^{3/8} \simeq 1$ (see Table I) and $P_{exh} << 1$ (see Fig. 3). Furthermore, it generally holds that $\xi \approx const$ [7]. With these approximations the scaling of n_S^{max} is completely determined by the first term in Eq. (6):

$$n_S^{max} \propto \frac{B_t^{5/16} q_\perp^{5/8}}{(qR)^{1/16}} \tag{23}$$

The coefficient of proportionality can be directly evaluated from Eq. (6). Owing to the weak dependence of the last term of Eq. (6) on T_D, the result is very insensitive to the precise value of T_D^{max}, and any value in the range between 5 and 20 eV gives, within about 10 per cent, the same result.

Numerical solutions of the full set of equations confirm the approximate consideration. The best fit is

$$n_S^{max} = 12.3 \frac{Q_\perp^{0.66} B_t^{0.33}}{(qR)^{0.06}} \tag{24}$$

where n_S^{max} is in $10^{19}\ cm^{-3}$, $Q_\perp = \frac{P_{in}}{4\pi R a \sqrt{\kappa}}$ in MW/m^2, B_t in T and R in m. Of course, the coefficient in Eq. (24) depends on the configuration.

Figure 9 gives a comparison of model predictions with the JET data base. In this database $\bar{n}$ is given instead of n_S (which was not available on JET) and therefore an assumption has to be made on the ratio $\bar{n}/n_S$. In these runs $\bar{n}/n_S = 5.5$ was adopted, where the value of 5.5 was derived by taking n_S from point P_3 of Table I and the corresponding measured

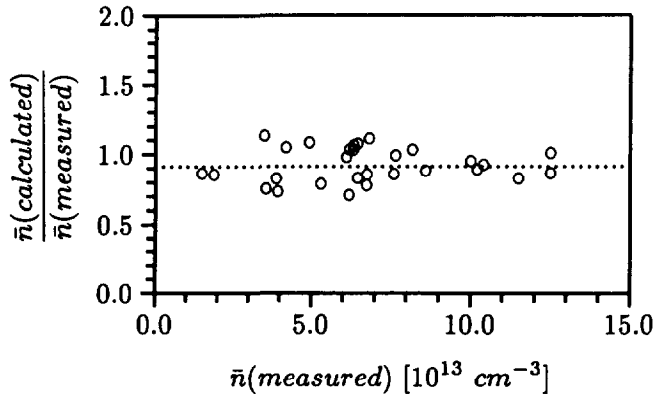

FIG. 9. *Calculated/measured maximum line average densities versus measured maximum line average density for beryllated JET density limit discharges. Range of parameter variation:* P_{in}*:* $0.9-21$ *MW;* B_t*:* $1.5-2.6$ *T;* q_c*:* $1.7-6.2$.

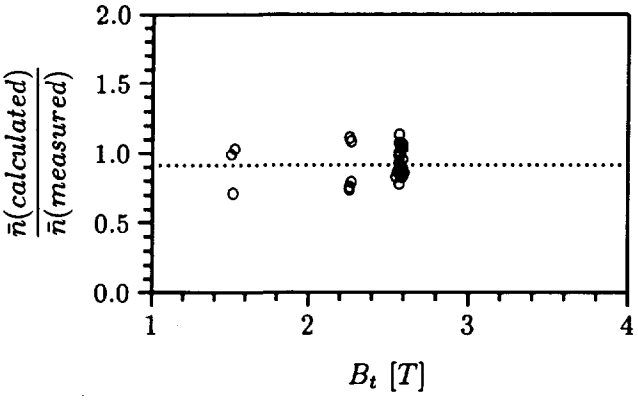

FIG. 10 *Same as Fig. 9, but the abscissa is the toroidal field.*

value of $\bar{n}$. It is assumed that $\bar{n}/n_S$ is a discharge independent constant.

As Fig. 5 shows, P_{rad} increases very rapidly near the limit and it is difficult to correlate its value precisely with the density maximum or the onset of marfes. Therefore, P_{rad} was calculated according to Eq. (21) instead of using the measured radiation losses, which results in a better fit. The remaining scatter is still associated with radiation and mainly results from the limited accuracy of the Z_{eff}-data. Figure 9 shows good quantitative agreement between experiment and simulation.

Perpendicular SOL transport is one of the most uncertain elements in SOL modelling and is difficult to determine directly. In the present model the B_t-dependence of n_S^{max} results entirely from the B_t-dependence of the Bohm-type perpendicular transport adopted, and the B_t-dependence in Eqs (23) and (24) provides a good test of this assumption. Figure 10 shows $\bar{n}(calculated)/\bar{n}(measured)$ versus B_t for the same database as in Fig. 9. Data are only available for three different B_t-values, but there is no indication of a deviation from the predicted B_t-scaling.

6. COMMENTS ON DISRUPTIVE VS NON-DISRUPTIVE DENSITY LIMITS

We begin by drawing a connection between the analysis of the non-disruptive density limit experiments in JET, performed in the beryllium limiter configuration and analyzed in this paper, and the earlier disruptive DL experiments in the carbon wall/carbon limiter JET configuration, analyzed be Wesson et al. [3]. In the beryllium case, the reduction of the edge density subsequent to formation of the marfe, as described by SOL theory, causes the marfe to extinguish, while in the C case it does not. The reasons for this must be found in a quantitative theory of the marfe itself and are beyond the scope of our SOL analysis. However, in the carbon machine case, where P_{rad} continues to increase after the onset of the marfe, the SOL theory predicts that for the trajectories shown in Figs 8 and 9, both n_S and T_D go towards zero, leading to detachment. The events subsequent to detachment, which lead to disruption, are then described by the model of Wesson et al. [3]. Thus, the SOL-based picture developed in this paper also describes the transition to detachment in the carbon machine case and should be regarded as a complementary part of the full story of the disruptive density limit in that case.

Secondly, we comment on the existence of local maxima in the curve n_S vs T_D for fixed $q_\perp$. In Ref. [7] a model is proposed where the disruption is associated with such local maxima. In this model the disruption occurs when the plasma is still in contact with the plates, as seems to be the case in ASDEX [4]. One might ask whether this situation may also exist in JET or other limiter tokamaks.

Figure 8 shows that $n_s(T_D, q_\perp)$ at constant $q_\perp$ is monotonic for the JET discharges under consideration. The shape of this curve is entirely determined by the last term of Eq. (6). Besides the explicit T_D-dependence, it depends on T_D through P_{exh} and the impurity radiation term. Noting that $\xi \simeq const$ and $\gamma \simeq const$, one concludes that in the ideal limit case, where $\int_0^L dz Q_{imp} = 0$ and $P_{exh} = 0$,

a maximum always exists, because n_S vanishes at $T_D = 0$ and $T_D = \infty$. A local maximum arises if s_w in Eq. (17) is sufficiently small. For shot 20845, for instance, this is the case if s_w is less than about 0.04 (the exact number depending somewhat on P_{in}). Impurity radiation losses from the SOL according to Eq. (18) support the formation of local maxima and, if the situation is marginal, even relatively small contributions may help to create a maximum [7]. In JET beryllium discharges, since impurity radiation losses are negligible and $s_w \simeq 0.1$, local maxima certainly never occur. Even in the case of a carbonized machine with an s_w of about half of that of beryllium, one seems to be above the threshold.

7. SUMMARY AND CONCLUSIONS

The density limit in JET beryllated limiter discharges shows a number of novel features in that it is a non-disruptive, refuelling type limit which is associated with a complicated time evolution of the edge parameters. The paper quantitatively describes the mechanism leading to an edge density maximum and explains the resistance to refuelling and the periodic occurrence of marfes. A scaling relation for the maximum density is derived and is demonstrated to be an excellent fit to the empirical data.

The limit is a bound of the edge density and the analysis is based on a model of the SOL of a limiter discharge. Formally, an upper bound for the edge density results from additional constraints which restrict the accessible part of the otherwise unbounded edge solution space. The relevant constraints are the relation between the edge density n_S and power flux $q_\perp$ into the SOL, provided by bulk radiation under quasi-steady-state conditions, and the fixing of the gas rate after the onset of marfes.

ACKNOWLEDGEMENTS

The authors gratefully acknowledge stimulating discussions with their JET and NET colleagues. Comments by J. Wesson clarified crucial issues. Valuable discussions with W. Eckstein, G. Haas and C. H. Wu on aspects relating to recycling are also gratefully acknowledged.

REFERENCES

[1] LOWRY, C. G., CAMPBELL, D. J., GOTTARDI, N., LAWSON, K., VLASES, G., et al., in Controlled Fusion and Plasma Heating (Proc. 17th Europ. Conf. Amsterdam, 1990), Vol. 14B, Part I, European Physical Society (1990) 339.

[2] STÄBLER, A., NIEDERMEYER, H., LOCH, R., MERTENS, V., MÜLLER, E. R., SÖLDNER, F. X., WAGNER, F., and the ASDEX, NI and Pellet Teams, in Controlled Fusion and Plasma Physics (Proc. 16th Eur. Conf. Venice, 1989), Vol. 13B, Part I, European Physical Society (1989) 23.

[3] WESSON, J. A., GILL, R. D., HUGON, M., SCHÜLLER, F. C., SNIPES, J. A., WARD, D. J., et al., Nucl. Fusion **29** (1989) 641.

[4] STÄBLER, A., McCORMICK, K., MERTENS, V., MÜLLER, E. R., NEUHAUSER, J., NIEDERMEYER, H., et al., to be published in Nuclear Fusion.

[5] POST, D. E., BORRASS, K., CALLEN, J. D., COHEN, S. A., CORDEY, J. G., ENGELMANN, F., et al., ITER Physics, ITER Documentation Series **21**, International Atomic Energy Agency, Vienna (1991).

[6] KURODA, T., VIEIDER, G., AKIBA, M., ANTIPENKOV, G., ARAKI, M., BAKER, C., et al., ITER Plasma Facing Components, ITER Documentation Series **30**, International Atomic Energy Agency, Vienna (1991).

[7] BORRASS, K., Nucl. Fusion **6** (1991) 1035.

[8] SAMM, U. (Kernforschungsanlage Jülich GmbH, Institut für Plasmaphysik, Jülich), personal communication, 1990.

[9] HARRISON, M. F. A., HARBOUR, P. J., HOTSTON, E. S., Nucl. Techn./Fusion **3** (1983) 432.

[10] BEHRISCH, R., ECKSTEIN, W., in Physics of Plasma-Wall Interactions in Controlled Fusion (Post, D. E., Behrisch, R., Eds), Plenum Press, New York and London (1986).

[11] HEIFETZ, D., B., in Physics of Plasma-Wall Interactions in Controlled Fusion (Post, D. E., Behrisch, R., Eds), Plenum Press, New York and London (1986).

[12] HARRISON, M. F. A., in Physics of Plasma-Wall Interactions in Controlled Fusion (Post, D. E., Behrisch, R., Eds), Plenum Press, New York and London (1986).

[13] GIBSON, W. M., The Physics of Nuclear Reactions, Pergamon Press, Oxford (1980).

[14] McCORMICK, K., HYATT, A., KYRIAKAKIS, G., MÜLLER, E. R., NIEDERMEYER, H., STÄBLER, A., THOMAS, D., TSOIS, N., ASDEX and NI Teams, in Controlled Fusion and Plasma Heating (Proc. 17th Eur. Conf. Amsterdam, 1990), Vol. 14B, Part III, European Physical Society (1990) 1439.

[15] CLEMENT, S., TAGLE, J. A., ERENTS, S. K., De COCK, L., SARTORI, R., SAIBENE, G., J. Nucl. Mater. **176&177** (1990) 432.
[16] DIETZ, K. J., and the JET TEAM, Plasma Phys. Controll. Fusion **32** (1990) 837.

ANNEX

P.-H. REBUT, A. GIBSON, M. HUGUET, J.M. ADAMS[1], B. ALPER, H. ALTMANN, A. ANDERSEN[2], P. ANDREW[3], M. ANGELONE[4], S. ALI-ARSHAD, P. BAIGGER, W. BAILEY, B. BALET, P. BARABASCHI, P. BARKER, R. BARNSLEY[5], M. BARONIAN, D.V. BARTLETT, L. BAYLOR[6], A.C. BELL, G. BENALI, P. BERTOLDI, E. BERTOLINI, V. BHATNAGAR, A.J. BICKLEY, D. BINDER, H. BINDSLEV[2], T. BONICELLI, S.J. BOOTH, G. BOSIA, M. BOTMAN, D. BOUCHER, P. BOUCQUEY, P. BREGER, H. BRELEN, H. BRINKSCHULTE, D. BROOKS, A. BROWN, T. BROWN, M. BRUSATI, S. BRYAN, J. BRZOZOWSKI[7], R. BUCHSE[22], T. BUDD, M. BURES, T. BUSINARO, P. BUTCHER, H. BUTTGEREIT, C. CALDWELL-NICHOLS, D.J. CAMPBELL, P. CARD, G. CELENTANO, C.D. CHALLIS, A.V. CHANKIN[8], A. CHERUBINI, D. CHIRON, J. CHRISTIANSEN, P. CHUILON, R. CLAESEN, S. CLEMENT, E. CLIPSHAM, J.P. COAD, I.H. COFFEY[9], A. COLTON, M. COMISKEY[10], S. CONROY, M. COOKE, D. COOPER, S. COOPER, J.G. CORDEY, W. CORE, G. CORRIGAN, S. CORTI, A.E. COSTLEY, G. COTTRELL, M. COX[11], P. CRIPWELL[12], O. Da COSTA, J. DAVIES, N. DAVIES, H. de BLANK, H. de ESCH, L. de KOCK, E. DEKSNIS, F. DELVART, G.B. DENNE-HINNOV, G. DESCHAMPS, W.J. DICKSON[13], K.J. DIETZ, S.L. DMITRENKO, M. DMITRIEVA[14], J. DOBBING, A. DOGLIO, N. DOLGETTA, S.E. DORLING. P.G. DOYLE, D.F. DÜCHS, H. DUQUENOY, A. EDWARDS, J. EHRENBERG, A. EKEDAHL, T. ELEVANT[7], S.K. ERENTS[11], L.G. ERIKSSON, H. FAJEMIROKUN[12], H. FALTER, J. FREILING[15], F. FREVILLE, C. FROGER, P. FROISSARD, K. FULLARD, M. GADEBERG, A. GALETSAS, T. GALLAGHER, D. GAMBIER, M. GARRIBBA, P. GAZE, R. GIANNELLA, R.D. GILL, A GIRARD, A. GONDHALEKAR, D. GOODALL[11], C. GORMEZANO, N.A. GOTTARDI, C. GOWERS, B.J. GREEN, B. GRIEVSON, R. HAANGE, A. HAIGH, C.J. HANCOCK, P.J. HARBOUR, T. HARTRAMPF, N.C. HAWKES[11], P. HAYNES[11], J.L. HEMMERICH, T. HENDER[11], J. HOEKZEMA, D. HOLLAND, M. HONE, L. HORTON, J. HOW, M. HUART, I. HUGHES, T.P. HUGHES[10], M. HUGON, Y. HUO[16], K. IDA[17], B. INGRAM, M. IRVING, J. JACQUINOT, H. JAECKEL, J.F. JAEGER, G. JANESCHITZ, Z. JANKOVICZ[18], O.N. JARVIS, F. JENSEN, E.M. JONES, H.D. JONES, L.P.D.F. JONES, S. JONES[19], T.T.C. JONES, J.-F. JUNGER, F. JUNIQUE, A. KAYE, B.E. KEEN, M. KEILHACKER, G.J. KELLY, W. KERNER, A. KHUDOLEEV[21], R. KONIG, A. KONSTANTELLOS, M. KOVANEN[20], G. KRAMER[15], P. KUPSCHUS, R. LÄSSER, J.R. LAST, B. LAUNDY, L. LAURO-TARONI, M. LAVEYRY, K. LAWSON[11], M. LENNHOLM, J. LINGERTAT[22], R.N. LITUNOVSKI, A. LOARTE, R. LOBEL, P. LOMAS, M. LOUGHLIN, C. LOWRY, J. LUPO, A.C. MAAS[15], J. MACHUZAK[19], B. MACKLIN, G. MADDISON[11], C.F. MAGGI[23], G. MAGYAR, W. MANDL[22], V. MARCHESE, G. MARCON, F. MARCUS, J. MART, D. MARTIN, E. MARTIN, R. MARTIN-SOLIS[24], P. MASSMANN, G. MATTHEWS, H. McBRYAN, G. McCRACKEN[11], J. McKIVITT, P. MERIGUET, P. MIELE, A. MILLER, J. MILLS, S.F. MILLS, P. MILLWARD, P. MILVERTON, E. MINARDI[4], R. MOHANTI[25], P.L. MONDINO, D. MONTGOMERY[26], A. MONTVAI[27], P. MORGAN, H. MORSI, D. MUIR, G. MURPHY, R. MYRNÄS[28], F. NAVE[29], G. NEWBERT, M. NEWMAN, P. NIELSEN, P. NOLL, W. OBERT, D. O'BRIEN, J. ORCHARD, J. O'ROURKE, R. OSTROM, M. OTTAVIANI, M. PAIN, F. PAOLETTI, S. PAPASTERGIOU, W. PARSONS, D. PASINI, D. PATEL, A. PEACOCK, N. PEACOCK[11], R.J.M. PEARCE, D. PEARSON[12], J.F. PENG[16], R. PEPE DE SILVA, G. PERINIC, C. PERRY, M. PETROV[21], M.A. PICK, J. PLANCOULAINE, J.-P POFFÉ, R. PÖHLCHEN, F. PORCELLI, L. PORTE[13], R. PRENTICE, S. PUPPIN, S. PUTVINSKII[8], G. RADFORD[30], T. RAIMONDI, M.C. RAMOS DE ANDRADE, R. REICHLE, J. REID, S. RICHARDS, E. RIGHI, F. RIMINI, D. ROBINSON[11], A. ROLFE, R.T. ROSS, L. ROSSI, R. RUSS, P. RUTTER, H.C. SACK, G. SADLER, G. SAIBENE, J.L. SALANAVE, G. SANAZZARO, A. SANTAGIUSTINA, R. SARTORI, C. SBORCHIA, P. SCHILD, M. SCHMID, G. SCHMIDT[31], B. SCHUNKE, S.M. SCOTT, L. SERIO, A SIBLEY, R. SIMONINI, A.C.C. SIPS, P. SMEULDERS, R. SMITH, R. STAGG, M. STAMP, P. STANGEBY[3], R. STANKIEWICZ[32], D.F. START, C.A. STEED, D. STORK, P.E. STOTT, P. STUBBERFIELD, D. SUMMERS, H. SUMMERS[13], L. SVENSSON, J.A. TAGLE[33], M. TALBOT, A. TANGA, A. TARONI, C. TERELLA, A TERRINGTON, A TESINI, P.R. THOMAS, E. THOMPSON, K. THOMSEN, F. TIBONE, A. TISCORNIA, P. TREVALION, B. TUBBING, P. VAN BELLE, H. VAN DER BEKEN, G. VLASES, M. VON HELLERMANN, T. WADE, C. WALKER, R. WALTON[31], D. WARD, M.L. WATKINS, N. WATKINS, M.J. WATSON, S. WEBER[34], J. WESSON, T.J. WIJNANDS, J. WILKS, D. WILSON, T. WINKEL, R. WOLF, D. WONG, C. WOODWARD, Y. WU[35], M. WYKES, D. YOUNG, I.D. YOUNG, L. ZANNELLI, A. ZOLFAGHARI[19], W. ZWINGMANN

[1] Harwell Laboratory, UKAEA, Harwell, Didcot, Oxfordshire, UK.
[2] Risø National Laboratory, Roskilde, Denmark.
[3] Institute for Aerospace Studies, University of Toronto, Downsview, Ontario, Canada.
[4] ENEA Frascati Energy Research Centre, Frascati, Rome, Italy.
[5] University of Leicester, Leicester, UK.
[6] Oak Ridge National Laboratory, Oak Ridge, TN, USA.
[7] Royal Institute of Technology, Stockholm, Sweden.
[8] I.V. Kurchatov Institute of Atomic Energy, Moscow, Russian Federation.
[9] Queens University, Belfast, UK.
[10] University of Essex, Colchester, UK.
[11] Culham Laboratory, UKAEA, Abingdon, Oxfordshire, UK.
[12] Imperial College of Science, Technology and Medicine, University of London, London, UK.
[13] University of Strathclyde, Glasgow, UK.
[14] Keldysh Institute of Applied Mathematics, Moscow, Russian Federation.
[15] FOM-Institute for Plasma Physics "Rijnhuizen", Nieuwegein, Netherlands.
[16] Institute of Plasma Physics, Academia Sinica, Hefei, Anhui Province, China.
[17] National Institute for Fusion Science, Nagoya, Japan.
[18] Soltan Institute for Nuclear Studies, Otwock/Świerk, Poland.
[19] Plasma Fusion Center, Massachusetts Institute of Technology, Boston, MA, USA.
[20] Nuclear Engineering Laboratory, Lappeenranta University, Finland.
[21] A.F. Ioffe Physico-Technical Institute, St. Petersburg, Russian Federation.
[22] Max-Planck-Institut für Plasmaphysik, Garching, Germany.
[23] Department of Physics, University of Milan, Milan, Italy.
[24] Universidad Complutense de Madrid, Madrid, Spain.
[25] North Carolina State University, Raleigh, NC, USA.
[26] Dartmouth College, Hanover, NH, USA.
[27] Central Research Institute for Physics, Budapest, Hungary.
[28] University of Lund, Lund, Sweden.
[29] Laboratorio Nacional de Engenharia e Tecnologia Industrial, Sacavem, Portugal.
[30] Institute of Mathematics, University of Oxford, Oxford, UK.
[31] Princeton Plasma Physics Laboratory, Princeton University, Princeton, NJ, USA.
[32] RCC Cyfronet, Otwock/Świerk, Poland,
[33] Centro de Investigaciones Energéticas, Medioambientales y Tecnológicas, Madrid, Spain.
[34] Freie Universität, Berlin, Germany.
[35] Insitute for Mechanics, Academia Sinica, Beijing, China.